Astronomy & Astrophysics manuscript no. output
July 15, 2026

Open cluster remnants in the *Gaia* epoch

I. NGC 1901, Ruprecht 3, Ruprecht 31, and ESO 426 SC26⋆

J. Latorre-Soto[1], C. Moni Bidin[1], D. González-Díaz[1], and G. Carraro[2]

[1] Instituto de Astronomía, Universidad Católica del Norte, Av. Angamos 0610, Antofagasta, Chile
[2] Dipartimento di Fisica e Astronomia, Università di Padova, Vicolo Osservatorio 3, I-35122, Padova, Italy

Received xxx, 2025; accepted xxx, 2025

ABSTRACT

Context. Most Galactic stars are born in large groups or stellar clusters, whose final stage before complete dissolution into the stellar field is a collection of a handful of stars, most of which are binaries, called open cluster remnants (OCR).
Aims. This study aims to determine whether the potential OCR candidates Ruprecht 3, Ruprecht 31, and ESO 426 SC26 are true star clusters by characterising their member stars based on kinematic and parallax data and studying their behaviour relative to the stellar background.
Methods. We used independent radial velocity measurements of thirty-eight stars from the FEROS and FIDEOS spectrographs, as well as precise astrometry from *Gaia* DR3.
Results. The radial velocity analysis shows a relatively low number of binary stars among our selected targets. Furthermore, the analysis of parallaxes, proper motions, and radial velocities shows no evidence of a kinematically and spatially consistent stellar group in the analysed fields. Additionally, we find that the original overdensity measurements are driven only by bright stars, as there is no excess of faint stars within the observed regions. We tested our methods using the well-known OCR NGC 1901.
Conclusions. We conclude that none of our three candidates are true OCRs but most likely asterisms. NGC 1901 is a 500±100 Myr-old cluster remnant located 418±6 pc from the Sun composed of no more than 20-25 stars within a 10′ radius from the centre.

Key words. (Galaxy:) open clusters and associations: general – (Galaxy:) open clusters and associations: individual: NGC1901 – Galaxy: stellar content

1. Introduction

It is generally accepted that the vast majority of field stars in the Milky Way are born within star clusters (see e.g. Lada & Lada 2003; Hopkins 2013). Upon formation, these structures gradually dissolve, allowing their constituent stars to escape into the field at a rate that depends both on the number of member stars and on the distance from the Galactic centre. The early theoretical works of Ambartsumian (1938) and Spitzer Jr (1940) showed that star clusters cannot evaporate completely, and remnants of a few stars may remain. Shorter-lived open clusters should theoretically leave behind small residual structures called open cluster remnants (OCRs). These consist of just a few dozen stars that survive the dissolution processes (Van Den Berk et al. 2007; Kouwenhoven et al. 2010; Moeckel & Clarke 2011; Reipurth & Mikkola 2012).

Early *N*-body simulations showed that the evaporation rate of open clusters starts slowly, then gradually accelerates, and slows again in the later stages of dynamical evolution (Von Hoerner 1960, 1963; Aarseth 1967; van Albada 1968). Later studies revealed more characteristics typical of OCRs, such as: *i*) a large fraction of binaries or multiple star systems; *ii*) a paucity of low-mass stars, which are the first to evaporate from the cluster; *iii*) a lifespan of several gigayears, which indicates a stable remnant (de La Fuente Marcos 1997; de la Fuente Marcos 1998). All of these characteristics distinguish OCRs from very low-mass open clusters.

Open cluster remnants (OCRs) are nearly indistinguishable from the field, making them very difficult to identify and study. This has led to an unsatisfactory situation in which the final phases of the cluster evolution are very well understood only in theory, while observational evidence is lacking. Attempts to identify OCRs date back to van Albada (1968) and Lodén (1987, 1988, 1993), and later extensive lists of potential OCRs have since been proposed in the literature (see e.g. Bica et al. 2001; Pavani & Bica 2007; Pavani et al. 2011). However, most of them have not survived deeper kinematical and spectroscopic analyses and have turned out to be mere asterisms (Stefanik et al. 1997; Baumgardt 1998; Odenkirchen & Soubiran 2002; Villanova et al. 2004; Carraro et al. 2005; Moni Bidin et al. 2010; Cantat-Gaudin & Anders 2020). Some authors have claimed confirmation of certain candidates (e.g. Pavani et al. 2001; de la Fuente Marcos et al. 2013; Angelo et al. 2019), but so far only one object has been uniformly recognised as genuine OCR in the literature (NGC 1901 Pavani et al. 2001; Pavani & Bica 2007; Carraro et al. 2007; Cantat-Gaudin & Anders 2020; Kos et al. 2018; Angelo et al. 2019).

Candidate OCRs are initially identified by slight overdensities in the number of stars compared to the Galactic field (see Lodén 1987, 1988, 1993, for early studies), which follow a distinctive sequence in colour-magnitude diagrams (CMDs,

⋆ Based on observations made with ESO Telescopes at the La Silla Paranal Observatory under programme ID 086.D-0963, and on observations collected by UCN at the ESO 1m telescope at the ESO La Silla Observatory.

Article published by EDP Sciences, to be cited as https://doi.org/10.1051/0004-6361/202658968

Bica et al. 2001; Pavani & Bica 2007). However, proper motions and parallaxes must also be consistent. These criteria are especially difficult to evaluate in crowded fields due to the low number of member stars. Despite these challenges, interest has increased in recent years due to the role that cluster evaporation plays in the formation of field stars in the Galactic disc (Carraro 2002, 2006; Villanova et al. 2004; Moni Bidin et al. 2010; Pavani et al. 2011). With the third data release (DR3) from the *Gaia* mission (Gaia Collaboration 2016), which includes precise measurements of proper motions, parallaxes, and multi-epoch radial velocities (RVs), a new era has begun in the study of OCRs has begun.

In this study, we revisit three high-likelihood OCRs: Ruprecht 3, Ruprecht 31, and ESO 426 SC26. These relatively compact concentrations of stars were proposed by Pavani & Bica (2007) as OCR candidates. The authors selected the members primarily based on photometric data from the Two Micron All Sky Survey (2MASS; Skrutskie et al. 2006), obtaining distance, age, and reddening through isochrone fitting. Angelo et al. (2019) confirm the OCR nature of all three objects, although different conclusions have been drawn in the literature for Ruprecht 3. Our study aims to determine whether our three OCR candidates behave as true stellar clusters based on kinematic and parallax data from Gaia DR3. We also aim to determine the number of binary or multiple systems within each candidate using RV measurements from different epochs. We included NGC 1901 in our analysis to test our methods on a previously-confirmed, well-known, genuine OCR.

2. Observations and data reduction

We selected the target stars from the 2MASS photometry as the brightest objects fitting the isochrones presented in Pavani & Bica (2007). We collected echelle spectra of thirty-eight stars in the field of our three OCR candidates between December 18-22, 2010 with the Fiber-fed Extended Range Optical Spectrograph (FEROS; Kaufer et al. 1999) on the MPG/ESO 2.2-m telescope at the La Silla Observatory. Exposure times ranged between 100 and 2700 s, according to the target magnitude, resulting in a signal-to-noise ratio of S/N≈20-60. We assigned the second fibre to the sky background, which we subtracted from the target spectra during data reduction. We acquired a set of second-epoch spectra of lower quality (S/N≈10-30) for the six brightest stars with 3600s exposures using the Fibre Dual Echelle Spectrograph instrument (FIDEOS; Vanzi et al. 2018) on the ESO 1-m telescope also at the La Silla Observatory, on 31 March 2023 and 1 April 2023. A sky fibre was not available with FIDEOS. During the observations, a one-quarter Moon was above the horizon but always more than 60° from the targets, and we expected no significant background contamination. In addition, we used the Collection of Elemental Routines for Echelle Spectra pipeline (CERES Brahm et al. 2017), which correctly estimates and manages systematics in RV measurements caused by a bright background. We used these results to confirm that our RV measurements were not affected by the lack of sky subtraction during data reduction.

We reduced the FEROS data with both the dedicated FEROS data reduction system (DRS) and with standard IRAF[1] routines. As discussed in de la Fuente Marcos et al. (2013), we found no substantial differences between the results and eventually adopted the DRS-reduced and order-merged spectra for our analysis. These were reduced to the 3500–7500 range Å and normalised with IRAF tasks. We removed cosmic rays by means of a sigma-clipping algorithm implemented in a Python-based script developed in this work. We reduced the FIDEOS spectra with CERES, which included the removal of cosmic rays and continuum normalisation.

[1] IRAF (Image Reduction and Analysis Facility) is distributed by the National Optical Astronomy Observatories, which are operated by the Association of Universities for Research in Astronomy, Inc., under cooperative agreement with the National Science Foundation.

Table 1. Comparison of the RVs of our FIDEOS targets from the *Gaia* catalogue, the values returned by the CERES pipeline, and our IRAF results.

ID	*Gaia* km s^{-1}	IRAF km s^{-1}	CERES km s^{-1}
Ruprecht 3			
1	54.0±0.2	54.1±0.4	53.99±0.01
2	45.7±0.2	45.5±0.8	45.90±0.03
Ruprecht 31			
1	28.1±1.8	−5.8±3.2	54.39±0.28
2	-	3.6±4.6	14.8±0.30
4	−5.9±0.2	−5.7±0.2	−6.09±0.01
ESO 426 SC26			
6	21.1±0.2	21.5±0.1	21.19±0.01

We complemented our spectroscopic data with proper motion, parallax, and multi-epoch average RVs from the *Gaia* DR3 catalogue. We downloaded information for all *Gaia* DR3 sources within 18′ from the centre of ESO 426 SC26 indicated in Pavani & Bica (2007), and 12′ from the centre of Ruprecht 3 and Ruprecht 31. We also retrieved similar *Gaia* DR3 data for NGC 1901, up to 10′ from its centre, although this cluster was not the target of new spectroscopic observations.

3. Spectroscopic measurements

3.1. Radial velocities

We measured the RVs of the target stars by cross-correlating (Simkin 1974; Tonry & Davis 1979) our spectra with synthetic templates extracted from the synthetic library of Coelho (2014). We selected templates with solar metallicity and no alpha-enhancement, and effective temperatures between 4500 K and 20000 K. We repeated each RV measurement while varying the template temperature to identify the best match to the object spectrum, as indicated by a higher peak of the cross-correlation (CC) function and a lower measurement error. We cross-correlated most targets with synthetic spectra with log g = 4.0, a value typical for main sequence (MS) objects, but we used log g = 2.0 for cool stars, and this improved the results. However, previous investigations have shown that a slight mismatch between the object and the template does not cause systematic errors, although it may slightly enhance the resulting random uncertainties (Morse et al. 1991; Moni Bidin et al. 2011).

We employed the IRAF `fxcor` task to calculate the CC function and to estimate the position of its peak by means of a Gaussian fit of its highest portion. We used a parabolic function when the peak profile was too far from Gaussian. We found that the formal error returned by `fxcor` is a factor of two lower when a parabolic fit is used. Hence, to keep the uncertainties consistent for all targets, we multiplied the error by two when a parabolic fit was used. Table A.1 presents the results of our RV measurements, together with *Gaia* data.

The CERES pipeline automatically measured the RVs of the FIDEOS targets during data reduction. Table 1 lists the results and compares them with the values extracted from the *Gaia* catalogue and with our IRAF measurements. The CERES RVs closely match both alternative estimates, except for the two hot stars Ruprecht 31-#1 and Ruprecht 31-#2. In fact, CERES does not include appropriate templates to handle hot-star spectra and, as a consequence, the RVs derived for hot objects are not reliable. The errors returned by CERES are one order of magnitude smaller than those obtained with the `fxcor` IRAF task. However, the data do not indicate that CERES errors are underestimated, because the differences between CERES and *Gaia* values are small and are fully accounted for by *Gaia* uncertainties.

The measurements obtained with FEROS and FIDEOS spectra agree in all cases except for the aforementioned two hot stars. The FEROS errors are noticeably smaller, although we used the same method and templates and both instruments provide a similar resolution. The difference is attributed to the much lower spectral S/N achieved with FIDEOS.

3.2. Metallicities

The chemical composition is another powerful tool that, combined with kinematic information, can indicate the presence of a coherent structure (e.g. Moni Bidin et al. 2010). We therefore inspected a list of ~150 iron lines relatively free of blending between 5400 and 6800 Å in each FEROS spectrum and measured their equivalent widths whenever a line was clearly detected and not saturated. However, the number of available lines was often too small to derive stellar atmospheric parameters (effective temperature T_{eff}, surface gravity log(g), and microturbulence v_t). We therefore adopted the photometric T_{eff} and log(g) from the *Gaia* catalogue for all stars and fixed v_t to a typical value depending on log(g) (1.5 and 2.0 km s^{-1} for the MS and giant stars, respectively). After removing spectra of too low quality (S/N≤30), hot stars (whose optical spectra contained no iron lines), and a few stars with no atmospheric parameters in *Gaia* catalogue, we were left with only two stars in Ruprecht 3 and three in Ruprecht 31. This sample is too small to add any useful information to the kinematic analysis. In ESO 426 SC26 we measured $\left[\frac{Fe}{H}\right]$ for seven objects, but we obtained values between −0.50 and −0.15 dex, within 2.4σ of each other. This is compatible both with a general field population and with a stellar cluster. These results are inconclusive and do not add information to the kinematical results. We therefore excluded the chemical study from further analysis in this work.

3.3. RV variable stars

The *Gaia* RVs reported in Table A.1 are averages of several measurements, between 15 and 20 for most of our stars, over a period of three years. The associated uncertainties are the statistical errors on the mean, which depend on the dispersion of the individual measurements. Intrinsic RV variability can enhance this value well beyond typical observational errors because it introduces an intrinsic spread. However, this also increases with magnitude and with decreasing colour, as shown in Fig. 1, because the measurement uncertainties are larger for fainter stars and bluer objects. As a consequence, an anomalously high *Gaia* error on the mean could suggest that a target star is a binary, but it is not necessarily direct evidence.

Among the six FIDEOS targets, Ruprecht 31-#1 is clearly a binary star because the *Gaia*, FEROS, and FIDEOS results differ well beyond the measurement errors. Ruprecht 31-#2 is also most likely a binary because, although it was not targeted by *Gaia*, the RVs measured with FEROS and FIDEOS are noticeably different. In this context, we performed all measurements with the same algorithm and templates, thus minimising systematics between the two data sets. The lower boundary of the FIDEOS spectra is at 4100 Å, which means that for hot stars such as Ruprecht 31-#2, only two Balmer lines are available for RV measurements. However, we verified that the difference between the two estimates remains unchanged even when limiting the FEROS CC to the same wavelength range available for FIDEOS. The other four stars targeted by FIDEOS are likely single stars, because *Gaia*, FEROS, and FIDEOS measurements differ by ~1 km s^{-1} at most, and the *Gaia* uncertainties are very small (0.2 km s^{-1}), suggesting a very low dispersion of *Gaia* measurements between epochs.

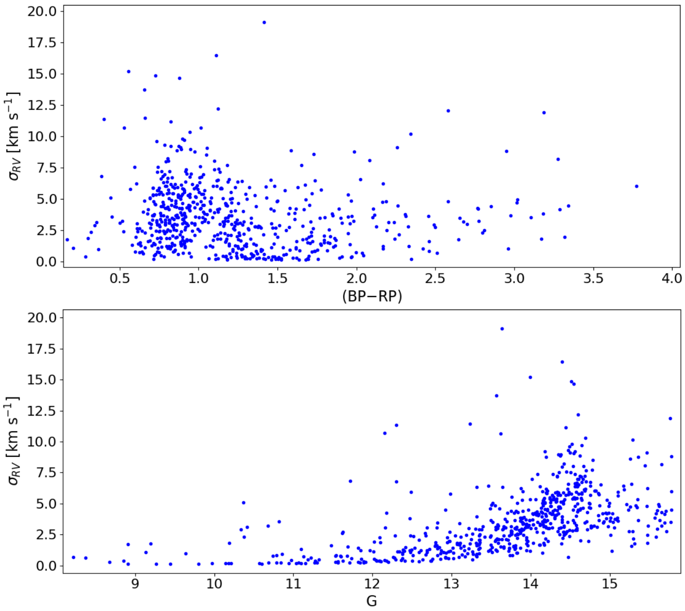

Fig. 1. *Gaia* error on the mean RV as a function of stellar colour (BP-RP; *top*) and G magnitude (*bottom*).

Of the 32 stars observed with FEROS but not with FIDEOS, two have no RV reported in the *Gaia* catalogue (Ruprecht 31-#8 and Ruprecht 31-#9), and our single-epoch measurements are not sufficient to study possible RV variations. The FEROS RV of 11 targets differs from the *Gaia* average by less than 1σ and/or 0.5 km s^{-1}, and those of seven more by less than 2σ and/or 1.5 km s^{-1}. In addition, their *Gaia* uncertainties are small, indicating that the *Gaia* measurements are also stable. The only exception is Ruprecht 3-#6, whose *Gaia* error is very large. We conclude that these seventeen stars are most likely single objects, while Ruprecht 3-#6 is a binary star whose single-epoch FEROS measurement happened to be close to the systemic RV by chance.

The stars Ruprecht 3-#5, Ruprecht 31-#7, Ruprecht 31-#11, ESO 426 SC26-#4, and ESO 426 SC26-#11 are clear binary systems because their FEROS measurement differs from the *Gaia* average by more than 5σ and 8 km s^{-1}, and their *Gaia* uncertainties are unusually large for their magnitude and colour. The nature of the remaining seven stars is more uncertain. The difference between the FEROS RVs and the *Gaia* average is limited for these stars (3.5-5.5 km s^{-1}), but large compared to the

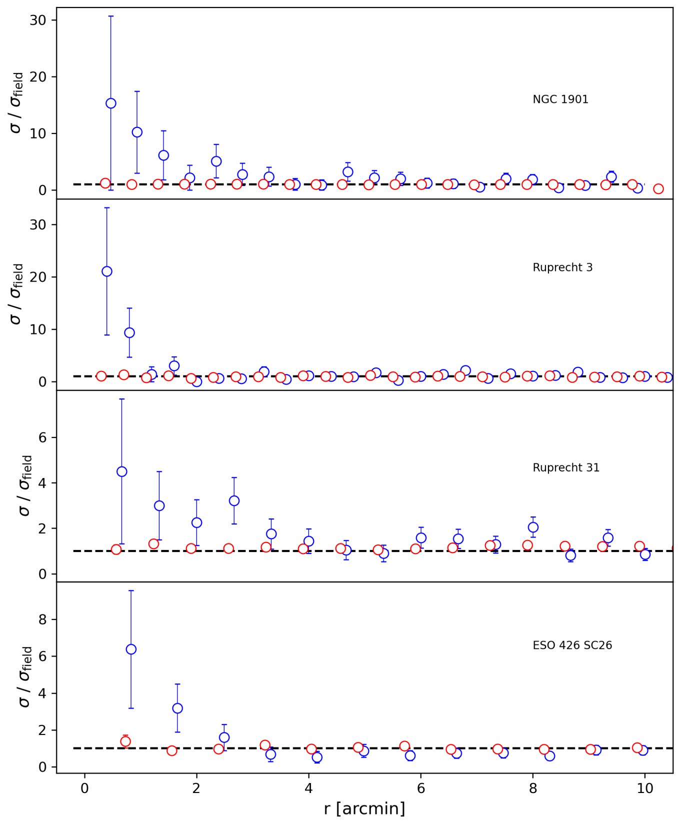

Fig. 2. Radial density profile of the candidate OCRs. The blue and red symbols show the stellar density for stars with G≤15 and G≥15, respectively.

FEROS errors ($\geq 4\sigma$). They generally have large *Gaia* uncertainties, which could be explained by their faint magnitudes.

4. *Gaia* database

All four OCR candidates stand out from the Galactic background as local over-densities of bright stars. Hence, we first studied these clumps of bright stars, looking for a group of objects with similar kinematic properties and distance. If found, these would serve as seeds for identifying additional cluster members at fainter magnitudes. We also ran an automatic code on the *Gaia* data to search for stars with coherent properties that may have escaped the initial analysis. We begin our analysis with the test case of NGC 1901.

4.1. NGC 1901

NGC 1901 is a well-known OCR, confirmed by spectroscopic and astrometric data in previous independent studies. We therefore used it to test the efficiency of our analysis, the detectability of true OCRs, and their behaviour in *Gaia* DR3 data.

The *Gaia* data show an overdensity of bright (G≤15) stars at the position of NGC 1901, extending up to 2.′5 from the centre, as shown in the top panel of Fig. 2. This overdensity is composed of 17 stars, 12 in excess of the general background density estimated at r≥ 4′, with a statistical significance of 5.5σ. The top panel of Fig. 3 shows the *Gaia* proper motions and parallax of these seventeen bright stars. Within this area, we identify a group of three objects with extremely similar proper motions and parallaxes, clearly visible at $\pi \approx 2.4$ mas. We report on their *Gaia* data in the first three lines of Table 2. We took the metallicities from the *Gaia*-based catalogue of Anders et al. (2022). Their RVs are also coincident. A fourth star (#4 in Table 2) is also part of this group because its larger parallax is still compatible within the large uncertainty. At the distance of these stars, a proper motion of 1 mas yr^{-1} corresponds to a linear velocity of only 2 km s^{-1}, while the internal velocity dispersion in an OC is typically of the order of 1 km s^{-1} (e.g. Ikhsan et al. 2019; Kulesh et al. 2024). As a consequence, a dispersion in μ_α^* and μ_δ must be allowed well beyond the small *Gaia* errors. Two more objects should be considered possible members: star #14, whose velocity components closely match those of cluster stars despite its lower parallax, and star #15, whose properties are compatible with membership except for a slightly lower μ_α^*.

Having identified a handful of probable cluster stars within the overdensity area, we searched for more objects with similar properties in the complete *Gaia* catalogue. We find nine additional stars with μ_α^* and μ_δ within 2σ or 0.5 mas yr^{-1}, π within 2σ or 0.1 mas, and RV within 2σ of the mean values of the four stars (stars #5 to #13 in Table 2). One more object complies with these constraints but is classified only as a possible member due to its distinct metallicity (star #16). In general, we find 124 stars with $|\Delta\mathrm{RV}| < 20$ km s^{-1}, $|\Delta\mu_\alpha^*|,|\Delta\mu_\delta| < 10$ mas yr^{-1}, and $|\Delta\pi| < 1$ mas. However, despite these extremely weak constraints, only eight of them are found in the CMD close to the sequence formed by the 13 already identified members, with all the others being much fainter. We report these eight stars as possible members in Table 2 (objects #17 to #24). We find that the metallicities of the cluster members are all consistent within errors and very similar overall, while we find a larger spread between the stars identified as less likely members. The weighted mean metallicity of the cluster members is $\left[\frac{\mathrm{M}}{\mathrm{H}}\right] = -0.43 \pm 0.06$.

In conclusion, we clearly detect the OCR in *Gaia* data through the presence of 13 stars with very similar distance, kinematics, and metallicity. We note that Table 2 includes all 14 cluster members indicated by Carraro et al. (2007), although we reclassify five here as less probable members. We add seven fainter stars, in particular three highly probable members (stars #10 to #12).

4.2. Ruprecht 3

We find no group of stars with similar kinematic properties among our nine spectroscopic targets (see Table A.1) except, to some extent, stars #4, #6, and #9, which have relatively similar parallaxes and proper motions. We selected these targets from the potential members reported by Pavani & Bica (2007). Using these three objects as a seed to detect a kinematically coherent structure, we selected all stars in *Gaia* photometry with proper motion components within 0.5 mas yr^{-1} of those of the three stars and $\pi = 0.5 - 0.8$ mas. However, the 33 stars that we selected do not clump at the cluster position, nor do they form a clear sequence in the CMD, as shown in Fig. 4. Their spatial distribution and photometric properties are indistinguishable from those of field stars in the same parallax range.

Pavani & Bica (2007) detected a highly significant overdensity of stars at the position of Ruprecht 3, limited to within 1-2′ of the centre. Using *Gaia*'s deeper photometry, we confirm the existence of this overdensity, which is due to a clump of bright stars, as shown in the radial density profile in Fig. 2: a higher

Table 2. *Gaia* data for member stars in NGC 1901.

ID	RA	DEC	G	$(B-R)$	μ_α^* (mas yr^{-1})	μ_δ (mas yr^{-1})	π (mas)	RV (km s^{-1})	$[\frac{M}{H}]$ (dex)
					Members				
1	5:18:22.5	−68:28:01.6	10.19	0.30	2.47±0.02	12.73±0.02	2.40±0.02	0.9±1.8	−0.51 ± 0.23
2	5:18:12.0	−68:25:36.3	10.34	0.34	1.76±0.02	12.76±0.02	2.40±0.01	2.7±2.9	−0.61 ± 0.30
3	5:18:19.2	−68:26:25.1	12.48	0.74	1.58±0.02	12.86±0.02	2.39±0.01	1.4±1.1	−0.92 ± 0.36
4	5:18:29.5	−68:27:13.8	11.48	0.68	2.59±0.17	12.56±0.19	2.57±0.15	0.5±1.6	−0.54 ± 0.26
5	5:18:02.1	−68:21:19.5	9.22	0.26	1.87±0.02	12.82±0.02	2.46±0.01	-	−0.62 ± 0.17
6	5:18:52.9	−68:34:13.3	10.37	0.32	1.70±0.01	12.80±0.02	2.40±0.01	3.6±2.3	−0.41 ± 0.25
7	5:17:35.8	−68:21:47.1	10.82	0.45	1.84±0.01	12.79±0.02	2.41±0.01	5.9±3.6	−0.51 ± 0.30
8	5:18:42.7	−68:27:32.7	11.48	0.58	1.87±0.01	12.65±0.02	2.41±0.01	-	−0.53 ± 0.22
9	5:17:59.2	−68:31:27.7	10.41	0.35	1.78±0.02	12.28±0.02	2.43±0.02	5.5±3.1	−0.42 ± 0.16
10	5:16:37.5	−68:24:48.9	13.52	1.09	1.48±0.04	13.03±0.04	2.33±0.04	−1.6±3.5	−0.14 ± 0.15
11	5:19:54.1	−68:28:03.6	15.88	1.71	1.42±0.04	12.79±0.04	2.43±0.03	-	-
12	5:16:52.5	−68:30:13.9	16.12	1.82	1.51±0.05	12.77±0.05	2.36±0.04	-	−0.43 ± 0.06
13	5:19:10.7	−68:34:51.7	9.84	0.34	1.57±0.02	12.53±0.02	2.42±0.01	-	−0.20 ± 0.30
					Possible members				
14	5:18:03.3	−68:27:56.7	8.22	0.94	1.72±0.03	12.57±0.03	1.63±0.03	2.0±0.7	−1.67 ± 0.16
15	5:17:51.4	−68:26:08.3	13.40	1.02	−0.34±0.16	13.51±0.16	2.23±0.13	2.8±3.1	−0.92 ± 0.21
16	5:16:34.3	−68:26:59.2	17.31	2.40	1.68±0.09	12.68±0.08	2.50±0.06	-	−0.10 ± 0.01
17	5:17:23.0	−68:28:19.1	9.14	0.21	1.45±0.02	12.17±0.02	2.39±0.01	−3.6±1.1	−0.39 ± 0.23
18	5:19:05.2	−68:30:45.8	12.16	0.69	3.07±0.02	14.18±0.03	2.34±0.02	2.7±3.1	−0.36 ± 0.07
19	5:16:50.0	−68:30:31.3	15.85	1.71	8.96±0.04	13.83±0.04	2.11±0.03	-	+0.02 ± 0.04
20	5:19:22.6	−68:27:23.1	12.59	0.80	−1.69±0.05	13.73±0.06	2.04±0.05	2.9±1.1	−0.79 ± 0.39
21	5:19:21.4	−68:19:30.3	17.54	2.23	3.55±0.08	13.07±0.10	1.45±0.07	-	-
22	5:17:45.9	−68:20:46.5	15.77	1.73	−1.50±0.03	20.86±0.04	2.65±0.03	-	−0.65 ± 0.17
23	5:19:51.1	−68:24:55.6	14.12	1.18	1.51±0.02	17.82±0.02	2.86±0.02	16.0±3.2	−0.70 ± 0.16
24	5:18:16.7	−68:25:10.4	11.22	0.65	1.72±0.02	9.47±0.02	2.73±0.01	18.1±0.6	−0.20 ± 0.10

central density within the inner 1′ is clearly visible for stars with G≤15, while it is completely absent for fainter objects. However, owing to the general scarcity of bright sources, this overdensity comprises only eleven stars, approximately six more than the mean field stellar count, corresponding to only a 2σ excess under the assumption of a Poissonian statistic for the field fluctuations. Fig. 3 shows the kinematical properties of these eleven stars, except for #3, which falls outside the plot due to its large parallax. A group of four objects with $\pi \approx 0.65$ mas, $\mu_\alpha^* \approx -2.5$ mas yr^{-1}, and $\mu_\delta \approx 2.0$ mas yr^{-1} is visible. However, this group includes the same stars(#4, #6, and #9) analysed above, and we find that they do not indicate the presence of an OCR.

4.3. Ruprecht 31

There are no similarities in the kinematical properties of our eleven spectroscopic targets that indicate the presence of an OCR. *Gaia* photometry detects a clump of sixteen bright (G≤15) stars within r≤ 2.′5 from the position of Ruprecht 31 indicated by Pavani & Bica (2007), as shown in Fig 2, while fainter stars do not clump at all at that position. This overdensity of bright stars stands out from the background with a significance of only $\approx 2.8\sigma$. It includes all our spectroscopic targets reported in Table A.1, except #8 and #9, which are excluded because they are fainter than our magnitude cut (G≤15).

Star #2 has no *Gaia* astrometry, so we exclude it from further analysis. Interestingly, four of the remaining 15 objects have similar RV (61-68 km s^{-1}), including the spectroscopic targets #3, #5, and #6 in Table A.1, plus an additional star not targeted in this work (RV=66.9±1.5 km s^{-1}). However, Fig. 3 shows the kinematical properties of these fifteen stars, which do not show any clear similarity: the stars are scattered over a wide range of parallaxes, and their proper motion components differ significantly. Hence, we find no kinematically coherent group of stars among the bright objects that clump at the position of Ruprecht 31.

4.4. ESO 426 SC26

Our observations of ESO 426 SC26 were more extensive than for the other two clusters: we targeted 18 stars, 60% more than in Ruprecht 31 and twice the number of targets observed in Ruprecht 3. One star in the *Gaia* catalogue that was not observed in our spectroscopic runs is located only 10.′′8 from target #15. Its magnitude G=13.33, parallax $\pi = 2.59 \pm 0.01$ mas, proper motion $(\mu_\alpha^*, \mu_\delta) = (-0.40 \pm 0.01, 17.36 \pm 0.01)$ mas yr^{-1}, and RV=40.9 ± 1.6 km s^{-1} are almost identical to those of object #15. From their distance and photometry we deduce that the mass of these two stars is approximately 0.9 $M_\odot$, and their physical separation is 4150 ± 20 AU. However, no other star in the *Gaia* catalogue shares the same astrometric properties as these two stars, so these must be regarded as a possible wide binary rather than part of a stellar system.

As with both Ruprecht 3 and Ruprecht 31, *Gaia* photometry shows a relevant overdensity (3.7σ) at the position of ESO 426 SC26. This overdensity is formed by 14 stars brighter than G=15 in the inner 2′ from the centre, as shown in Fig. 2. This corresponds to 11 stars in excess of the mean field density. However, the *Gaia* parallaxes and proper motions of these 14 stars are highly dispersed, and we find no group with similar properties among them (Fig. 3).

From Table A.1, we find no group of stars with similar distances and kinematic properties, except possibly targets #6 and #16, whose proper motions and parallaxes are only marginally similar. To investigate this further, we selected stars with μ_α^* and μ_δ within 1 mas yr^{-1} of their values and parallaxes in the range

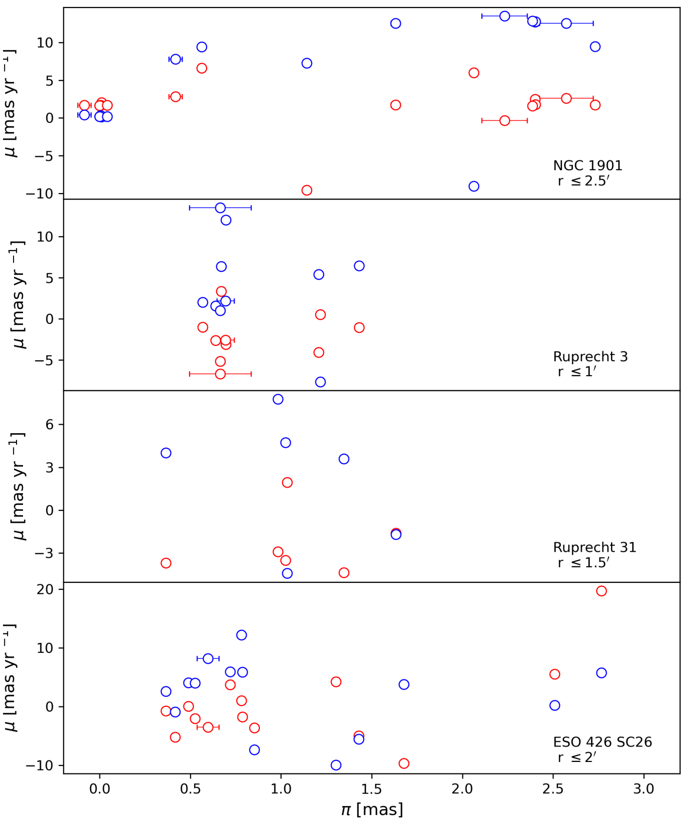

Fig. 3. Proper motion components μ_α^* (blue symbols) and μ_δ (red symbols) as a function of parallax, for bright stars (G≤15) within the radial distance indicated in each panel.

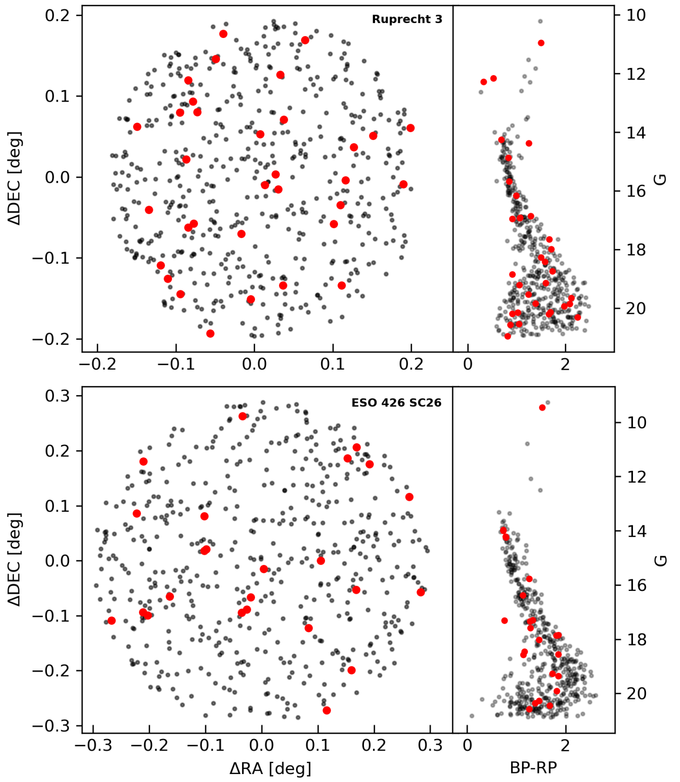

Fig. 4. Spatial distribution (*left subpanels*) and CMD (*right subpanels*) of stars with similar astrometric parameters (red dots) in the field of Ruprecht 3 (*top panel*) and ESO 426 SC26 (*bottom panel*), compared with all field stars in the same parallax range (grey dots).

π = 0.66 – 0.86 mas, as shown in Fig. 4. These 24 stars are scattered both spatially and in the CMD, and their distribution closely follows that of field stars in the same parallax range. In conclusion, we find no evidence for a stellar cluster in this field.

4.5. Overdensity search code

Angelo et al. (2019) used a decontamination algorithm to identify the most probable members of Ruprecht 3, Ruprecht 31, and ESO 426 SC26 using *Gaia* DR2 astrometric parameters. The authors reported 14 members for Ruprecht 3, 15 for Ruprecht 31, and 19 for ESO 426 SC26. We ran the algorithm described in Angelo et al. (2019), which follows similar procedures to those adopted in Dias et al. (2012, 2018), and Angelo et al. (2017), to identify cluster members using the updated *Gaia* DR3 astrometric parameters. In short, the algorithm divides the 3D astrometric space into grids whose cells contain stars in both the cluster and field regions, defined as the region beyond three times the cluster radius. The cell size is initially proportional to the mean uncertainties in each axis and then increases and decreases by one-third of the original value. In this way, the algorithm runs 27 different sets of grids. It computes a membership probability for those astrometric cells in which the stars in the cluster area are more concentrated than those in the field area (see Angelo et al. 2019, for more details). A visual inspection of the most likely members in the CMD reveals the presence of a group of stars consistent with a stellar cluster.

We tested the algorithm on known open clusters in both sparse and crowded fields and improved its performance. We found that the algorithm is sensitive to the sampling ranges used and the size of the grids. In several cases, the edges of the grids divide the group of cluster stars into different cells, thus significantly decreasing their statistical weight. To account for these effects, we introduced additional sets of grids to the algorithm, with the original cell size multiplied by a factor of 2.5; each cell was then increased and decreased by one-third of its size. We obtained the final probability value after running 729 different sets of grids, which makes the algorithm statistically more robust.

We first applied the procedure to the known OCR NGC 1901, and it correctly returned the 16 tightest member stars in astrometric space with high membership likelihoods. As expected, they form a clear MS in the CMD. Fig. 6 (bottom row) shows the results, where the yellow circles represent the stars with the highest probabilities. We also plot the target stars of Table 2 in the same figure, to illustrate the good agreement with the methodology.

We could not obtain similar results for the other three OCR candidates. Fig. 6 shows that the tightest group of stars in 3D astrometric space in the cluster area is very sparse, their distribution is not distinct from the field, and they do not form a clear sequence in the CMD. The comparison between the well-known OCR NGC 1901 and the other three candidates is particularly striking. As a second check, we carefully inspected the distribution in the proper motions and CMDs for each group of stars falling in bins of sizes of 0.1 mas and 0.2 mas in the parallax

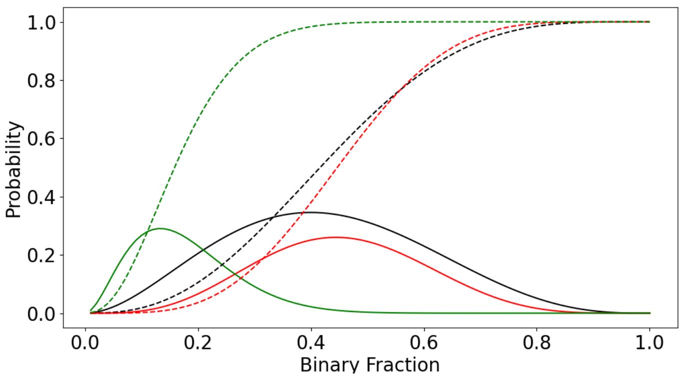

Fig. 5. Probability distribution (solid curves) and cumulative probability distribution (dashed curves) of the intrinsic binary fraction resulting from our spectroscopic study for Ruprecht 3 (red curves), Ruprecht 31 (black curves), and ESO 426 SC26 (green curves).

distribution within the cluster area. We find no evidence of any potential OCR stellar association.

5. Discussion

We analysed the properties of the stars in the field of four candidate OCRs, searching for evidence of a spatially and kinematically coherent group. We clearly detect NGC 1901 in every attempt. In contrast, we find no evidence of an OCR at the positions of Ruprecht 3, Ruprecht 31, and ESO 426 SC26.

Theoretical studies have shown that single stars are the first objects to evaporate from a dissolving cluster, leaving behind an OCR mainly composed of binary stars (de La Fuente Marcos 1997; de la Fuente Marcos 1998). Carraro et al. (2007) observationally confirmed this result, finding a binary fraction greater than 62% in the genuine OCR NGC 1901.

In our spectroscopic study, we detect two binaries out of five stars in Ruprecht 3, four out of nine in Ruprecht 31, and two out of fifteen in ESO 426 SC26 (last column of Table A.1). Fig. 5 shows the resulting probability and cumulative probability distributions as a function of the intrinsic binary fraction. The most probable fraction for Ruprecht 3 and Ruprecht 31 is ~40-45%, a value typical of intermediate-mass stars in the generic Galactic field (e.g. Duchêne & Kraus 2013; GRAVITY Collaboration et al. 2018). The probability distribution functions are broad because of the limited sample size, but there is only a 10% probability of a binary fraction higher than 65%. The results for ESO 426 SC26 are more constrained due the larger sample size, and indicate an even lower binary fraction. In conclusion, our spectroscopic analysis finds no evidence of the enhanced binary fraction that would be expected in the presence of an OCR, although due to the limited sample size, we cannot draw firm conclusions. However, we note that we did not target any of the candidates of Angelo et al. (2019) in our spectroscopic study, as we selected our targets from the list of Pavani & Bica (2007), which does not have stars in common with this more recent work.

NGC 1901 is extensively studied in the literature and to date is the only OCR that has been confirmed without controversy by all previous work (Pavani et al. 2001; Pavani & Bica 2007; Carraro et al. 2007; Cantat-Gaudin & Anders 2020; Kos et al. 2018; Angelo et al. 2019). We find that despite its ease of detection, it contains no more than 20-25 stars within 10′ of the centre. Carraro et al. (2007) and Kos et al. (2018) obtained similar results, finding 27 stars with membership probabilities higher than 70%, which are reduced to 23 objects when radial velocities are taken into account.

The mean distance of the 13 cluster members, taken from the Bailer-Jones et al. (2021) catalogue, is d=418 ± 6 pc, where the error corresponds to the standard deviation of the measurements. This result agrees with previous studies, although our uncertainty is smaller thanks to the high quality of the *Gaia* data. In contrast, the Anders et al. (2022) photometric metallicities reported in Table 2 are noticeably lower than previous estimates by Carraro et al. (2007, $[\frac{\mathrm{Fe}}{\mathrm{H}}] = -0.08$) and Kos et al. (2018, $[\frac{\mathrm{Fe}}{\mathrm{H}}] = -0.27$). However, the spectroscopic measurement of Carraro et al. (2007) was based only on the star HD35294 (star #14 in Table 2), whose cluster membership is doubtful due to its low parallax. Similarly, the cluster age is uncertain if this star is not considered a cluster member, as this is the only object evolved off the MS. We fitted a Padova isochrone (Bressan et al. 2012) to the sequence of the most probable cluster members, assuming the previously derived cluster distance and solar metallicity, which is reasonable for an object so close to the Sun. We find that a 500 Myr isochrone fits the cluster sequence reasonably well for a reddening E($BP-RP$)= 0.07 ± 0.01, which implies E($B-V$)= 0.05 ± 0.01, in line with the Carraro et al. (2007) estimate (E($B-V$)= 0.04 ± 0.01). The 500 Myr model fails to fit the presumed subgiant star HD35294, but it follows the MS distribution well when accounting for the fact that the two brightest stars are binaries (Carraro et al. 2007). Including HD35294 leads to an older age of 600 Myr, as shown in Fig. 7. We therefore conclude that our best estimate of the age of the cluster is 500±100 Myr, where the error is derived from the isochrones that still fit the upper MS reasonably well. Our results indicate an age older than the 400±100 Myr found by Carraro et al. (2007), but still younger than the 690±80 Myr obtained by Kos et al. (2018), who also find a higher reddening of E($B-V$)=0.09.

The internal velocity dispersion of NGC 1901 deserves particular attention because it could directly affect the fate and lifetime of the cluster. While Cantat-Gaudin & Anders (2020) find a low value of about 1 km s^{-1}, Kos et al. (2018) measure a much higher value (2.80±0.27 km s^{-1}), and they claim that, with this high dispersion, the cluster will not survive its next crossing of the Galactic plane within 18 Myr. The fact that the only OCR unequivocally confirmed so far could be so short-lived is notable, as it contrasts with the expected stable structure with a lifetime of several Gyr (de La Fuente Marcos 1997; de la Fuente Marcos 1998).

The observed RV dispersion in the *Gaia* data is σ_{obs}=2.6 km s^{-1} and is essentially the same whether only confirmed members are considered or five additional possible members are included (Table 2). This is of the same order of magnitude as the average measurement error (2.2 and 2.5 km s^{-1} respectively, in the two cases), suggesting a very low internal dispersion. We estimated the internal RV dispersion σ_{int} by calculating the probability of the RV of each star individually, as if extracted from a Gaussian distribution centred on the average cluster RV, with σ equal to the quadratic sum of σ_{int} and the measurement error. Combining these probabilities for all stars, we then adjusted σ_{int} to find the value that best reproduces the observations. We obtain $\sigma_{\mathrm{int}} = 1.1 \pm 1.0$ km s^{-1} for the eight confirmed members, and $\sigma_{\mathrm{int}} = 1.0 \pm 0.9$ km s^{-1} when we include the five additional candidates.

We further studied the relation between σ_{obs} and σ_{int} by simulating samples of 13 stars, that is, the eight cluster members plus the five possible ones. We obtained their intrinsic RV by

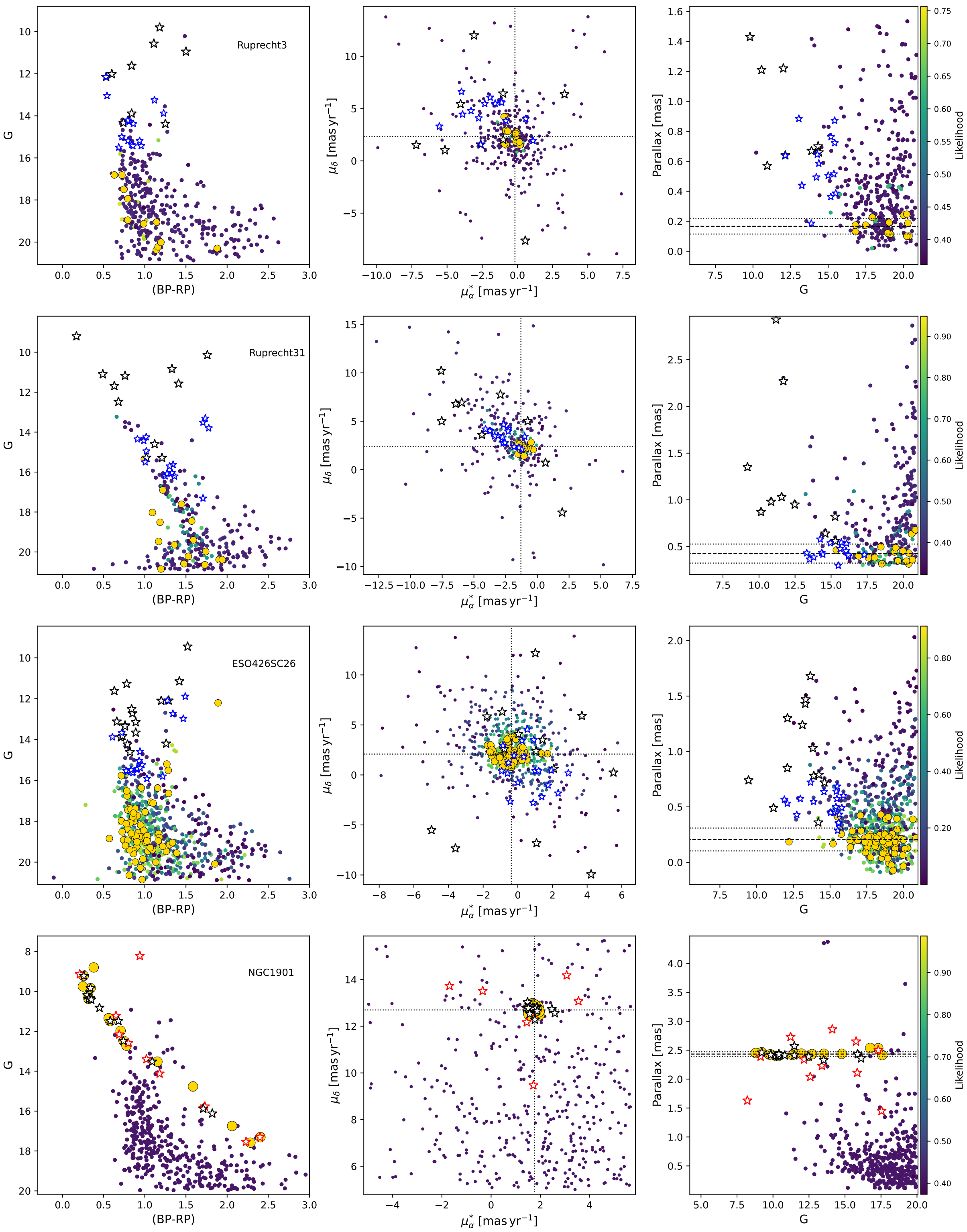

Fig. 6. Colour-magnitude diagram (G vs BP-RP; *left column*), proper motion diagram (*middle column*), and parallax vs G-magnitude (*right column*), of stars within the cluster area of the four OCR candidates. The colour bar represents the membership probability for the tightest stars in the astrometric space (see text). The dashed lines show the mean proper motion values and parallaxes for star with likelihoods > 86%. The dotted lines in the parallax vs G-magnitude panel indicate the standard deviation of these data. Our targets, extracted from Pavani & Bica (2007), are shown as open black stars, while the cluster candidates suggested by Angelo et al. (2019) are superimposed as blue stars. The black and red star symbols in the bottom panel represent the members and possible members of NGC 1901 in Table 2, respectively.

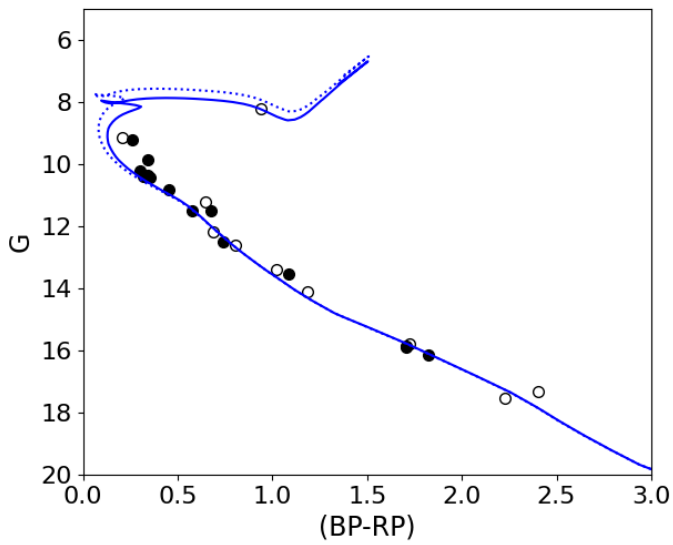

Fig. 7. *Gaia* CMD of the stars in the field of NGC 1901. The black dots show the positions of the cluster members (stars #1 to #13 in Table 2), while the empty symbols indicate the lower-probability candidate members (#14 to #24 in Table 2). Theoretical isochrones of 500 Myr (dotted curve) and 600 Myr (full curve) are also shown.

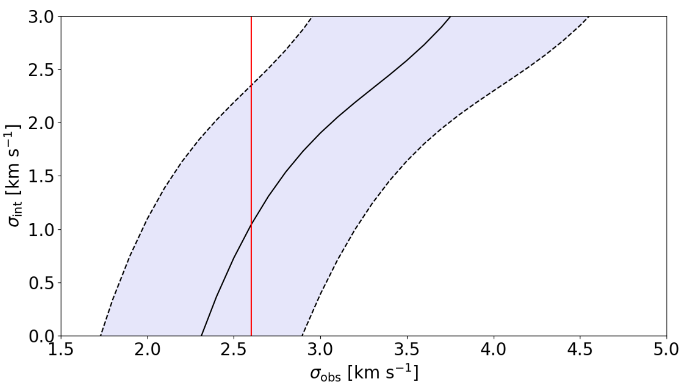

Fig. 8. Simulated relation between the intrinsic velocity dispersion of the cluster NGC 1901 (σ_{int}), and the observed dispersion (σ_{obs}). The grey band shows the $\pm 1\sigma$ standard deviation. The vertical red line indicates the observed σ_{obs} from *Gaia* data.

extracting 13 random values from a normal distribution with dispersion σ_{int}. We then applied a normally distributed observational error to each RV independently, adopting for each star an error equal to the 13 values reported in Table 2. We repeated the procedure ten thousand times for each value of σ_{int} in the range 0.1-3.0 km s^{-1}, finally retrieving the average σ_{obs} and its standard deviation as a function of σ_{int}. Figure 8 shows the results, with the red line marking the real observed RV dispersion. This test confirms that the most probable intrinsic RV dispersion is low (1.1 km s^{-1}), but the result is not very conclusive because within 1σ a value as high as σ_{int}=2.6 km s^{-1} is allowed. In conclusion, the high RV dispersion proposed by Kos et al. (2018) is unlikely, and our results favour the scenario of a stable, kinematically cold structure, but the uncertainties are too large for a firm conclusion. Our test also indicates that this large uncertainty on σ_{int} is only partially due to the limited sample size: even if we artificially increase it to 30 stars, the 1σ standard deviation on σ_{int} would still be 0.9 km s^{-1}. The main source of uncertainty here is the large *Gaia* errors, which are inflated by binarity: if they are reduced to 1.0 km s^{-1} in the simulations, the 1σ uncertainty on σ_{int} decreases to ∼ 0.7 km s^{-1}. As a consequence, our result could be improved by resolving the RV curves of the cluster members to derive their systemic velocity.

Ruprecht 3 is an object extensively studied and highly debated in the literature: while Pavani et al. (2003), Bonatto et al. (2004), Pavani & Bica (2007) and Angelo et al. (2019) concluded that it is a true OCR, many other studies argue against this claim (Piatti et al. 2017; Bica et al. 2019; Cantat-Gaudin & Anders 2020). We also find that no kinematically coherent structure is present in the field and that this object should be regarded as an asterism. In particular, we find that the thirteen stars proposed by Pavani et al. (2003) as possible cluster members have no properties in common (parallax, proper motion, or radial velocity), and they are therefore physically unrelated. Ruprecht 31 and ESO 426 SC26, on the contrary, were studied only by Pavani & Bica (2007) and Angelo et al. (2019), who both claimed the existence of a real OCR but, as for Ruprecht 3, they propose very diverse distance and kinematical properties for them, based on different lists of cluster members, with no stars in common. Our results for these two objects are the same as for Ruprecht 3.

The *Gaia* catalogue reveal an overdensity of bright stars at the literature position of these three clusters, although they are only mildly significant (between 2 and 3.7σ), and due to at most ten bright stars. We find no coherence between the *Gaia* astrometric data of these bright stars, indicating that these overdensities are only random fluctuations of the field density. Fainter stars, on the other hand, do not clump at all at the cluster positions.

In addition to investigating the properties of the brightest stars, we also ran an automatic code to detect clumps and overdensities in the 3D astrometric space (proper motion and parallax). Fig. 6 shows that the results are very different for NGC 1901 and the other three objects. The stars in the field of NGC 1901 are sharply divided into two categories: those with an extremely high probability of being cluster members (> 90%) and those whose probability is negligible. In contrast, this is not the case for the other three clusters, where the stars are continuously distributed at all values, and many stars with intermediate probability (50-80%) are found. Thus, the overdensities detected by the code do not emerge clearly from the field, and the high-probability stars appear to be drawn from the general field distribution. In addition, the stars identified by the code as the most probable members are all at faint magnitudes (in general G> 16), which contradicts the fact that these OCR candidates are characterised by a clump of bright stars. The distance of these overdensities (between 2.5 and 5.0 kpc) is also too large compared to the distance derived by Pavani & Bica (2007, ∼1 kpc for the three objects) and Angelo et al. (2019, between 2 and 2.3 kpc).

The code we used in Sect. 4.5 is conceptually identical to the algorithm employed by Angelo et al. (2019), and it is surprising that our results differ so much from theirs. However, Angelo et al. (2019) allowed the proposed cluster members to span a very large interval in proper motion and parallax: the dispersion of their proper motion, for example, is $\pm 1.0 - 1.5$ mas yr^{-1} in each component, which is 25-35 times the average *Gaia* DR2 errors. At the distances proposed in their work, these values translate into 9-14 km s^{-1}, which is a large velocity dispersion not compatible with a bound system. In contrast, we imposed more stringent constraints on the size of the clumps in kinematical space, compatible with *Gaia* errors and a cluster velocity dispersion of a few km s^{-1}. With these constraints, although *Gaia* DR3 errors are on average 30% smaller than DR2, we would not have detected the Angelo et al. (2019) clusters even using *Gaia* DR2 data. The differences in results are therefore mainly due to a different tolerance in the dispersions of the astrometric quantities of the member candidates.

6. Conclusions

Our results can be summarised as follows:

– We obtained RVs for thirty-eight stars previously associated with three OCR candidates: Ruprecht 3, Ruprecht 31 and ESO 426 SC 26. Only eight of them showed RV variability beyond their uncertainties, meaning that they are binaries.
– We tested our methodology to study the real nature of the OCR candidates using the well-known OCR NGC 1901. We find thirteen likely member stars and eleven additional possible members, forming a complete set of members for this cluster. We derive its distance as d=418 ± 6 pc and its age as 500±100 Myr. The RV dispersion is of the order of 1 km s^{-1}, suggesting that NGC 1901 is a stable, long-lived object, but the uncertainties are too large for a firm conclusion.
– We find no evidence of a true OCR in the fields of Ruprecht 3, Ruprecht 31, and ESO 426 SC 26. The kinematical properties of the targets are widely scattered and generally similar to those expected for field stars. Our density analysis shows that previous misidentifications of these fields as OCRs are due to clumps of bright stars, with statistical significance in the range 2-3.7σ. We conclude that these objects are asterisms.

Acknowledgements. We gratefully thanks the referee, W. Elsanhoury, for his very useful comments and suggestions. Part of this work was supported by the German *Deutsche Forschungsgemeinschaft, DFG* project number Ts 17/2–1. D.G.-D. gratefully acknowledge support from ANID /FONDO 2023 ALMA / 31230017.

References

Aarseth, S. 1967, Bulletin astronomique, 3, 105
Ambartsumian, V. 1938, Leningrad State Univ, 22, 19
Anders, F., Khalatyan, A., Queiroz, A. B. A., et al. 2022, A&A, 658, A91
Angelo, M. S., Santos, J. F. C., Corradi, W. J. B., & Maia, F. F. S. 2019, A&A, 624, A8
Angelo, M. S., Santos Jr., J. F. C., Corradi, W. J. B., Maia, F. F. S., & Piatti, A. E. 2017, Research in Astronomy and Astrophysics, 17, 4
Bailer-Jones, C. A. L., Rybizki, J., Fouesneau, M., Demleitner, M., & Andrae, R. 2021, AJ, 161, 147
Baumgardt, H. 1998, A&A, 340, 402
Bica, E., Pavani, D. B., Bonatto, C. J., & Lima, E. F. 2019, AJ, 157, 12
Bica, E., Santiago, B. X., Dutra, C. M., et al. 2001, Astronomy & Astrophysics, 366, 827
Bonatto, C., Bica, E., & Pavani, D. B. 2004, A&A, 427, 485
Brahm, R., Jordán, A., & Espinoza, N. 2017, Publications of the Astronomical Society of the Pacific, 129, 034002
Bressan, A., Marigo, P., Girardi, L., et al. 2012, MNRAS, 427, 127
Cantat-Gaudin, T. & Anders, F. 2020, A&A, 633, A99
Carraro, G. 2002, Astronomy & Astrophysics, 385, 471
Carraro, G. 2006, Bulletin of the Astronomical Society of India, vol. 34, Issue 2, p. 153, 34, 153
Carraro, G., de la Fuente Marcos, R., Villanova, S., et al. 2007, Astronomy & Astrophysics, 466, 931
Carraro, G., Dinescu, D. I., Girard, T. M., & van Altena, W. F. 2005, A&A, 433, 143
Coelho, P. R. T. 2014, Monthly Notices of the Royal Astronomical Society, 440, 1027
de La Fuente Marcos, R. 1997, Astronomy and Astrophysics, 322, 764
de la Fuente Marcos, R. 1998, Astronomy and Astrophysics, 333, L27
de la Fuente Marcos, R., de la Fuente Marcos, C., Bidin, C. M., Carraro, G., & Costa, E. 2013, Monthly Notices of the Royal Astronomical Society, 434, 194
Dias, W. S., Monteiro, H., Caetano, T. C., & Oliveira, A. F. 2012, A&A, 539, A125
Dias, W. S., Monteiro, H., Lépine, J. R. D., et al. 2018, MNRAS, 481, 3887
Duchêne, G. & Kraus, A. 2013, ARA&A, 51, 269
Gaia Collaboration. 2016, Astronomy & Astrophysics, 595, A1
GRAVITY Collaboration, Karl, M., Pfuhl, O., et al. 2018, A&A, 620, A116
Hopkins, P. F. 2013, MNRAS, 428, 1950
Ikhsan, M. I., Arifyanto, M. I., Aprilia, Hakim, M. I., & Soegiartini, E. 2019, in Journal of Physics Conference Series, Vol. 1231, Journal of Physics Conference Series (IOP), 012027
Kaufer, A., Stahl, O., Tubbesing, S., et al. 1999, The Messenger, 95, 8
Kos, J., de Silva, G., Buder, S., et al. 2018, MNRAS, 480, 5242
Kouwenhoven, M., Goodwin, S., Parker, R. J., et al. 2010, Monthly Notices of the Royal Astronomical Society, 404, 1835
Kulesh, M. V., Samirkhanova, A. E., Carraro, G., et al. 2024, AJ, 167, 212
Lada, C. J. & Lada, E. A. 2003, ARA&A, 41, 57
Lodén, L. 1987, in Astronomical Science Group of Ireland, Meeting, Trinity College, Dublin, Apr. 6, 1987 Irish Astronomical Journal (ISSN 0021-1052), vol. 18, Sept. 1987, p. 95-97., Vol. 18, 95–97
Lodén, L. 1988, Astrophysics and Space Science, Volume 142, Issue 1-2, pp. 177-179, 142, 177
Lodén, L. 1993, Astrophysics and Space Science (ISSN 0004-640X), vol. 199, no. 1, p. 165-167., 199, 165
Moeckel, N. & Clarke, C. J. 2011, Monthly Notices of the Royal Astronomical Society, 415, 1179
Moni Bidin, C., de La Fuente Marcos, R., de La Fuente Marcos, C., & Carraro, G. 2010, Astronomy & Astrophysics, 510, A44
Moni Bidin, C., Villanova, S., Piotto, G., & Momany, Y. 2011, A&A, 528, A127
Morse, J. A., Mathieu, R. D., & Levine, S. E. 1991, AJ, 101, 1495
Odenkirchen, M. & Soubiran, C. 2002, A&A, 383, 163
Pavani, D. B. & Bica, E. 2007, Astronomy & Astrophysics, 468, 139
Pavani, D. B., Bica, E., Ahumada, A. V., & Clariá, J. J. 2003, A&A, 399, 113
Pavani, D. B., Bica, E., Dutra, C. M., et al. 2001, A&A, 374, 554
Pavani, D. B., Kerber, L. d. O., Bica, E., & Maciel, W. J. 2011, Monthly Notices of the Royal Astronomical Society, 412, 1611
Piatti, A. E., Dias, W. S., & Sampedro, L. M. 2017, MNRAS, 466, 392
Reipurth, B. & Mikkola, S. 2012, Nature, 492, 221
Simkin, S. M. 1974, A&A, 31, 129
Skrutskie, M. F., Cutri, R. M., Stiening, R., et al. 2006, AJ, 131, 1163
Spitzer Jr, L. 1940, Monthly Notices of the Royal Astronomical Society, 100, 396
Stefanik, R. P., Caruso, J. R., Torres, G., Jha, S., & Latham, D. W. 1997, Baltic Astronomy, 6, 137
Tonry, J. & Davis, M. 1979, AJ, 84, 1511
van Albada, T. S. 1968, Bulletin of the Astronomical Institutes of the Netherlands, Vol. 19, p. 479, 19, 479
Van Den Berk, J., Portegies Zwart, S., & McMillan, S. 2007, Monthly Notices of the Royal Astronomical Society, 379, 111
Vanzi, L., Zapata, A., Flores, M., et al. 2018, MNRAS, 477, 5041
Villanova, S., Carraro, G., de la Fuente Marcos, R., & Stagni, R. 2004, A&A, 428, 67
Von Hoerner, S. 1960, Zeitschrift fur Astrophysik, 50
Von Hoerner, S. 1963, Z. Astrophys. 57, 47-82, 57

Appendix A: Data of spectroscopic targets

Table A.1. *Gaia* data and RV measurements of our spectroscopic targets.

ID	RA	DEC	G	$(B-R)$	μ_α^* (mas yr^{-1})	μ_δ (mas yr^{-1})	π (mas)	RV$_{\rm Gaia}$ (km s^{-1})	RV$_{\rm FEROS}$ (km s^{-1})	RV$_{\rm FIDEOS}$ (km s^{-1})	^{a}
					Ruprecht 3						
1	06:42:11.3	−29:27:32.4	9.80	1.18	−1.02±0.01	6.45±0.01	1.43±0.01	54.0±0.2	53.2±0.1	54.1±0.4	s
2	06:42:07.8	−29:27:07.2	10.57	1.11	−4.04±0.01	5.44±0.01	1.21±0.01	45.7±0.2	46.0±0.1	45.5±0.8	s
3	06:42:06.3	−29:27:15.8	11.62	0.84	−7.19±0.15	1.51±0.16	3.99±0.16	14.8±2.7	19.1±0.8	-	?
4	06:42:05.0	−29:27:36.4	10.95	1.50	−1.01±0.01	2.03±0.01	0.57±0.01	−0.2±0.2	−0.2±0.1	-	s
5	06:42:01.0	−29:27:40.3	12.02	0.60	0.56±0.02	−7.63±0.02	1.22±0.02	−12.5±2.0	−4.6±1.5	-	b
6	06:42:03.9	−29:26:30.8	12.15	0.53	−2.61±0.01	1.57±0.01	0.64±0.01	28.0±10.7	26.8±1.8	-	b
7	06:42:07.9	−29:27:17.3	14.33	0.74	−3.08±0.02	12.01±0.02	0.70±0.02	95.1±7.2	90.4±1.2	-	?
8	06:42:05.8	−29:26:21.5	13.89	0.84	3.35±0.01	6.37±0.01	0.67±0.02	33.5±2.9	37.0±0.3	-	?
9	06:42:08.6	−29:26:49.2	14.38	1.25	−5.15±0.02	1.02±0.02	0.66±0.02	32.1±3.0	36.2±0.1	-	?
					Ruprecht 31						
1	07:43:00.2	−35:35:21.8	9.20	0.17	−4.37±0.02	3.60±0.02	1.35±0.02	28.1±1.8	7.6±2.4	−5.8±3.2	b
2	07:43:03.8	−35:35:42.0	11.10	0.49	-	-	-	-	27.0±2.1	3.6±4.6	b
3	07:42:56.0	−35:36:09.7	10.84	1.33	−2.91±0.01	7.76±0.01	0.98±0.01	61.6±0.2	61.4±0.1	-	s
4	07:42:52.6	−35:36:58.0	10.14	1.76	−0.76±0.01	5.01±0.01	0.87±0.01	−5.9±0.2	−5.6±0.1	−5.7±0.2	s
5	07:42:55.7	−35:35:21.8	11.18	0.76	−8.97±0.02	40.74±0.02	2.93±0.02	61.0±0.5	60.8±0.3	-	s
6	07:43:00.8	−35:36:12.2	11.57	1.41	1.96±0.01	−4.42±0.01	1.03±0.01	68.2±0.3	68.2±0.1	-	s
7	07:42:52.6	−35:35:43.8	14.60	1.12	−7.58±0.02	10.21±0.02	0.64±0.02	50.8±12.2	58.8±0.9	-	b
8	07:42:59.2	−35:36:05.0	15.29	1.21	−5.96±0.02	6.93±0.02	0.56±0.02	-	74.9±1.0	-	?
9	07:43:03.3	−35:35:54.2	15.28	1.02	0.64±0.03	0.73±0.03	0.82±0.03	-	55.5±0.9	-	?
10	07:42:58.7	−35:33:41.8	11.69	0.63	−7.54±0.01	5.01±0.01	2.27±0.01	21.8±1.5	18.5±2.7	-	s
11	07:42:49.8	−35:34:36.5	12.48	0.68	−6.43±0.01	6.80±0.01	0.95±0.01	51.5±3.8	28.5±2.7	-	b
					ESO 426 SC26						
1	06:36:15.1	−30:49:59.5	11.15	1.42	0.03±0.02	4.08±0.02	0.49±0.02	57.5±0.2	57.9±0.1	-	s
2	06:36:14.1	−30:50:46.7	12.09	1.29	−3.60±0.01	−7.34±0.01	0.85±0.01	6.5±0.4	6.5±0.1	-	s
3	06:36:11.2	−30:50:08.9	12.72	0.85	19.72±0.01	5.74±0.01	2.77±0.01	96.1±1.3	94.9±0.6	-	s
4	06:36:11.3	−30:50:24.0	13.89	0.71	1.01±0.02	12.18±0.02	0.78±0.02	13.0±5.3	24.7±0.8	-	b
5	06:36:13.1	−30:47:47.0	12.51	0.84	1.05±0.01	2.38±0.01	2.90±0.01	65.3±0.8	64.0±0.2	-	s
6	06:36:26.2	−30:47:31.2	9.45	1.52	−0.90±0.01	6.32±0.01	0.74±0.01	21.1±0.2	21.3±0.1	21.5±0.1	s
7	06:36:04.5	−30:51:32.0	13.83	0.73	1.43±0.01	3.52±0.01	1.03±0.01	26.2±3.1	21.8±0.8	-	?
8	06:36:19.3	−30:53:03.1	12.10	1.20	4.23±0.01	−9.94±0.01	1.30±0.01	50.4±0.3	50.1±0.1	-	s
9	06:36:18.2	−30:53:20.0	13.31	0.76	−4.98±0.01	−5.52±0.01	1.43±0.01	3.7±1.8	5.0±0.2	-	s
10	06:36:20.3	−30:52:37.2	13.66	0.89	−9.66±0.01	3.79±0.01	1.68±0.01	50.8±2.4	49.2±0.2	-	s
11	06:36:25.3	−30:51:02.9	11.62	0.63	5.52±0.01	0.24±0.02	2.51±0.01	29.3±2.6	18.3±2.1	-	b
12	06:36:19.9	−30:51:30.6	14.20	1.26	−0.77±0.02	2.60±0.02	0.36±0.02	90.0±3.1	91.2±0.1	-	s
13	06:36:23.0	−30:52:04.1	14.62	0.82	3.70±0.02	5.90±0.02	0.72±0.02	23.0±7.2	19.5±0.1	-	?
14	06:36:27.1	−30:52:43.7	13.12	0.66	1.08±0.01	−6.82±0.01	1.24±0.01	32.7±2.3	33.2±0.3	-	s
15	06:36:37.0	−30:50:00.6	13.15	0.89	−0.23±0.01	17.28±0.01	2.60±0.01	38.3±1.6	39.4±0.2	-	s
16	06:36:17.7	−30:51:57.2	14.24	0.79	−1.78±0.02	5.85±0.02	0.79±0.02	63.3±4.2	57.9±0.1	-	?
17	06:36:32.2	−30:51:19.8	13.35	0.76	2.08±0.01	0.62±0.01	1.47±0.01	36.2±2.4	35.9±0.1	-	s
18	06:36:14.0	−30:56:07.1	11.27	0.78	6.03±0.01	32.45±0.01	2.54±0.01	50.8±0.4	50.9±0.2	-	s

Notes. [a] Flag for binarity: b = binary star; s = single star; ? = uncertain binarity.